



Cite this: *Chem. Commun.*, 2020, 56, 4571

Received 12th February 2020,  
Accepted 13th March 2020

DOI: 10.1039/d0cc01117g

rsc.li/chemcomm

# *In situ* generated nanozyme-initiated cascade reaction for amplified surface plasmon resonance sensing†

Xin Wang, Wenxin Lv, Jiahui Wu, Haiyin Li\* and Feng Li 

**A novel nanozyme-based surface plasmon resonance (SPR) sensor was successfully developed based on the target-induced *in situ* generation of AuNPs and a AuNP-guided cascade reaction, with  $\text{Hg}^{2+}$  as the target analyte.**

The surface plasmon resonance (SPR) technique has attracted worldwide attention in the field of bio-analytical chemistry and medical science due to its vibrant performance in the real-time monitoring of bio-molecular interactions.<sup>1–4</sup> In a SPR system, the SPR angle is highly dependent on the refractive index of a disk surface, which is dependent on the molecular weight of the immobilized bio-molecules.<sup>5,6</sup> However, most of the target biomolecules only have low molecular weights and ultralow expression levels in biological fluids, making the SPR angle shift tiny when they are immobilized on the disk.<sup>7–9</sup> Thus, it is imperative to propose novel SPR sensors for target biomolecules for highly sensitive biosensing. In this context, a large number of studies have been carried out, and these studies justified the great potential of nanomaterial-mediated amplification for diverse analyte biosensing.<sup>10–15</sup> However, the application of nanomaterials in a SPR system generally involves tedious preparation, strict conditions and functional modification, which consume large amounts of raw materials, generate large amounts of waste, and affect the activity of biomolecules, further influencing the diagnosis result.<sup>7,16–18</sup> A strategy to overcome these obstacles is to achieve the *in situ* formation of nanomaterials by using bio-molecules as templates.<sup>19–21</sup>

Nanozymes are a subclass of nanomaterials and can mimic the natural enzymes' structures and functions with low cost and high stability.<sup>22,23</sup> Nanozymes have been widely used in the diagnosis and treatment of diseases, environmental manipulation, and industrial catalysis. AuNPs are a kind of typical nanozymes and are a potential test kit for diverse analytes.<sup>24,25</sup> AuNPs catalyze

the hydrolysis or oxidation of substances into desired compounds, increase the refractive index when they are immobilized on a SPR disk, and thus can be employed to develop a signal-amplified SPR sensor. Several methods have been reported to develop AuNP-based SPR sensors with high sensitivity, such as pre-preparing AuNPs and modifying AuNPs with DNA and streptavidin.<sup>26–29</sup> However, presynthetic and modification methods are unfavourable due to the reasons mentioned above. More importantly, these sensors only employ the inherent nature of AuNPs to improve sensitivity, and the enzyme property is not involved. It is highly desirable to develop a nanozyme-based SPR sensor that does not require the presynthesis and modification of AuNPs and makes full use of the SPR effect and enzyme property of AuNPs to achieve output signal cascade amplification. However, no simple procedure to develop such a SPR sensor has been reported yet.

Herein, we propose a target-initiated nanozyme *in situ* generated strategy to develop a SPR sensor for the highly sensitive detection of  $\text{Hg}^{2+}$ , used as the target analyte. T30 on the SPR disk selectively captures  $\text{Hg}^{2+}$ , and the captured  $\text{Hg}^{2+}$  induces and accelerates the *in situ* formation of AuNPs based on its catalyzing reaction with  $\text{HAuCl}_4$  and  $\text{NH}_2\text{OH}$ .<sup>30</sup> The generated AuNPs not only enhance the SPR angle, but also catalyze tetramethylbenzidine (TMB, Fig. S1A, ESI†) into oxidized TMB (oxTMB, Fig. S1B, ESI†) due to their horseradish peroxidase (HRP)-like activity. oxTMB is deposited on the disk to increase the reflectivity, further increasing the SPR angle.<sup>31</sup> Based on the change in the SPR angle, a highly sensitive SPR sensor for  $\text{Hg}^{2+}$  is realized.

The key goal of this work in the development of a nanozyme-based SPR sensor is to control the formation of AuNPs with high HRP-like activity. To confirm this, a solution containing  $\text{HAuCl}_4$ ,  $\text{NH}_2\text{OH}$ , tween 80, and T30 in the absence/presence of  $\text{Hg}^{2+}$  was investigated. As depicted in Fig. S2A (ESI†), when  $\text{Hg}^{2+}$  was absent, the color slowly changed into red, which was validated using a UV-vis spectrum. The characterization results shown in Fig. S2B (ESI†) and Fig. S3 (ESI†) demonstrated that absorbance at 560 nm remained constant with the time increasing from 0 to 14 min, implying no generation of AuNPs.

College of Chemistry and Pharmaceutical Sciences, Qingdao Agricultural University, Qingdao, 266109, People's Republic of China. E-mail: lifeng@qau.edu.cn, lihaiyin@qau.edu.cn

† Electronic supplementary information (ESI) available. See DOI: 10.1039/d0cc01117g

Meanwhile, no aggregates were observed from the TEM image (Fig. S4A, ESI†). With a further increase in time, the absorbance elevated and reached a plateau at 28 min, implying the appearance of AuNPs, and thus, as shown in Fig. S4B (ESI†), 30 nm nanoparticles were determined. However, when  $\text{Hg}^{2+}$  was present, the color of the solution changed rapidly (Fig. S2C, ESI†), and the absorbance increased with the increase in time and levelled off at 7 min (Fig. S2D, ESI†). Meanwhile, there were many aggregates observed in the solution (Fig. S4C, ESI†). This is because  $\text{Hg}^{2+}$  was reduced by  $\text{NH}_2\text{OH}$  into liquid Hg, and the generated liquid Hg reacted with Au to form a Au–Hg amalgamation, which catalyzed the  $\text{HAuCl}_4\text{--NH}_2\text{OH}$  reduction reaction and acted as a nucleation agent to accelerate the formation of AuNPs. Moreover, it is worth noting that the time taken for the generation of AuNPs in the presence of  $\text{Hg}^{2+}$  is much less than that in the absence of  $\text{Hg}^{2+}$ , and the absorbance is much higher.

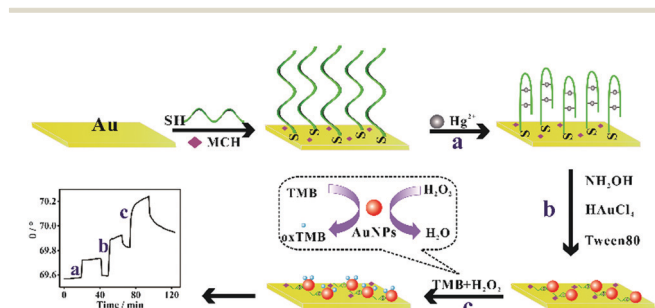
Further, the HRP-like activity of the generated AuNPs was investigated, and the diagram is shown in Fig. S5A and C (ESI†), respectively. It was reported that individual AuNPs have a relatively low HRP-like activity and  $\text{Hg}^{2+}$  can enhance the HRP-like activity of AuNPs.<sup>32</sup> Thus, AuNPs in the absence of  $\text{Hg}^{2+}$  cannot catalyze the oxidation of TMB into oxTMB, and the absorbance at 650 nm remained unchanged even if the time was prolonged to 240 s, accompanied by no change in color (Fig. S5B, ESI†). In the presence of  $\text{Hg}^{2+}$ , AuNPs efficiently catalyze the oxidation of TMB into oxTMB, accompanied by a deep blue color change and high absorbance (Fig. S5D, ESI†). From this context, it was inferred that the generation of AuNPs with HRP-like activity can be controlled by the absence/presence of  $\text{Hg}^{2+}$  and varying the reaction time, thus justifying the significant possibility of our strategy for nanozyme-based SPR sensor development.

The mechanism of the nanozyme-based SPR sensor for highly sensitive biosensing of  $\text{Hg}^{2+}$  is illustrated in Scheme 1. Here, T30 is modified with  $-\text{SH}$  at 5' and comprises 30 thymine, in which  $-\text{SH}$  contributes to immobilization on the SPR disk and the T sequences favour the selective and efficient capture of  $\text{Hg}^{2+}$ . In the absence of  $\text{Hg}^{2+}$ , T30 in 6-mercapto-1-hexanol (MCH)/T30/Au kept its configuration unvaried. As the generation of AuNPs is highly dependent on the amount of  $\text{Hg}^{2+}$ , there were no AuNPs formed, affording a slight change in the SPR angle. However, when  $\text{Hg}^{2+}$  was added, the coordination recognition of MCH/T30/Au by  $\text{Hg}^{2+}$  leads to its immobilization on the disk,

thereby resulting in the formation of abundant AuNPs. The produced AuNPs catalyze the oxidation of TMB into oxTMB. On the basis of the influence of AuNPs and oxTMB on refractive index, the significantly increased SPR angle was determined. Since the SPR angle is highly dependent on the generation of AuNPs, which depends on the amount of  $\text{Hg}^{2+}$ , the highly sensitive detection of  $\text{Hg}^{2+}$  can be readily achieved by using our proposed sensor.

To verify the propitious fabrication of the nanozyme-based SPR sensor, electrochemical impedance spectroscopy (EIS) was first carried out. A bare Au disk displayed a low electron-transfer resistance ( $R_{\text{et}}$ ) of  $\sim 440\ \Omega$ , as shown in Fig. 1A. After being sequentially modified with T30 and MCH,  $R_{\text{et}}$  increased to  $\sim 4463\ \Omega$  and  $\sim 5203\ \Omega$ , respectively, justifying the successful linkage of T30 and MCH to the Au disk. Further,  $\text{Hg}^{2+}$  capture led to a slight decrease in  $R_{\text{et}}$  due to the decrease in negative charge density. Upon treatment with  $\text{HAuCl}_4$ ,  $\text{NH}_2\text{OH}$ , and tween 80, the disk presented a significantly decreased  $R_{\text{et}}$ , confirming the formation of AuNPs and corresponding well to the fact that AuNPs possess high conductivity. Expectedly, some 60 nm nanoparticles were observed (Fig. 1E). When TMB and  $\text{H}_2\text{O}_2$  were further added, the disk showed an increased  $R_{\text{et}}$ , which was due to the deposition of oxTMB and its relatively low conductivity compared with that of AuNPs. Meanwhile, oxTMB/AuNPs/ $\text{Hg}^{2+}$ /MCH/T30/Au presented some irregular nanoparticles, whose diameter is larger than that of AuNPs/ $\text{Hg}^{2+}$ /MCH/T30/Au (Fig. 1F). Subsequently, cyclic voltammetry (CV) was employed to further investigate the step by step modification of the SPR disk. As shown in Fig. 1B, the Au disk presented large currents of 0.16 V and 0.26 V, respectively. Upon treatment with T30 or MCH or TMB +  $\text{H}_2\text{O}_2$ , all disks gave a smaller current compared with the previous one. Further,  $\text{Hg}^{2+}$  capture and AuNP formation led to an increase in current. These EIS and CV results firmly confirm that T30, MCH,  $\text{Hg}^{2+}$ , AuNPs, and oxTMB were successfully immobilized on the SPR disk.

To obtain direct insights into the gradual modification, SPR characterization was conducted (Fig. 1C). Immobilization of T30 and MCH led to an increase in SPR angle ( $\theta$ ), reflecting the



**Scheme 1** Schematic representation of the working principle of the nanozyme-based SPR sensor for highly sensitive biosensing of  $\text{Hg}^{2+}$ .

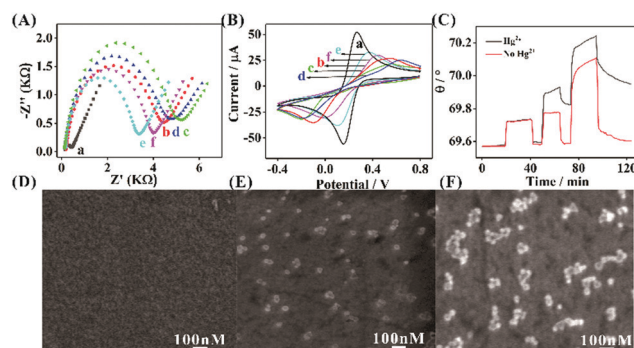


**Fig. 1** (A) EIS curves and (B) CV curves of bare Au disk (a), T30 (b), T30 + MCH (c), T30 + MCH +  $\text{Hg}^{2+}$  (d), T30 + MCH +  $\text{Hg}^{2+}$  + AuNPs (e), T30 + MCH +  $\text{Hg}^{2+}$  + AuNPs + oxTMB (f) modified SPR disks. The concentration of  $\text{Hg}^{2+}$  was 2000 pM. (C) SPR curves of the disk in the absence/presence of 2000 pM  $\text{Hg}^{2+}$ . SEM images of Au disk (D), AuNPs/2000 pM  $\text{Hg}^{2+}$ /MCH/T30/Au (E), and oxTMB/AuNPs/2000 pM  $\text{Hg}^{2+}$ /MCH/T30/Au (F).

change in refractive index. After the  $\text{Hg}^{2+}$  solution was injected and the disk was subsequently washed with water, a little change in  $\theta$  was observed. Upon the  $\text{Hg}^{2+}$ -induced AuNP generation,  $\theta$  shifted with  $\Delta\theta$  of  $0.23^\circ$  compared with that of MCH/T30/Au. Moreover,  $\Delta\theta$  further increased once TMB and  $\text{H}_2\text{O}_2$  were introduced, indicating the successful oxidation of TMB and deposition of oxTMB on the disk. Undoubtedly, the shifted SPR angle was due to the increased refractive index, justifying the feasibility of the *in situ* produced AuNP-mediated cascade amplification reaction.

To validate the response of our SPR sensor toward  $\text{Hg}^{2+}$  and the *in situ* prepared AuNP-initiated cascade reaction, SPR measurements were conducted. As shown in Fig. 1C, in the absence of  $\text{Hg}^{2+}$ , there was a slight shift in the  $\theta$  value when  $\text{HAuCl}_4$ ,  $\text{NH}_2\text{OH}$ , and tween 80 were added. This is because no AuNPs were formed and deposited on the SPR disk, subsequently leading to a similar angle to that of MCH/T30/Au. Nevertheless, when  $\text{Hg}^{2+}$  was added, no AuNPs were generated, and the  $\theta$  value changed from  $69.57^\circ$  to  $69.585^\circ$ . Undoubtedly,  $\text{Hg}^{2+}$  indeed can change the SPR angle, but  $\Delta\theta$  ( $0.015^\circ$ ) is negligible. When the AuNPs were formed,  $\theta$  increased from  $69.57^\circ$  to  $69.94^\circ$  with a  $\Delta\theta$  of  $0.37^\circ$ , which is much higher than that when the AuNPs did not form. The increase in  $\Delta\theta$  is a result of the formation of AuNPs and oxTMB on the disk, which obviously varied the reflectivity, subsequently contributing to an enhanced SPR angle. From these SPR results, it can be concluded that the target-initiated *in situ* generation of AuNPs and AuNP-catalyzed oxTMB formation can considerably enhance the SPR angle and lead to an improvement in  $\text{Hg}^{2+}$  sensing performance.

The structure of T30 plays a critical role in specifically recognizing target  $\text{Hg}^{2+}$ , and it was thus studied. Two other ssDNAs (A30 and B30) modified with  $-\text{SH}$  have different sequences to that of T30 and were applied as contrast substances in the development of the SPR sensor. The diagram illustration of the A30 or B30-participated SPR sensor for  $\text{Hg}^{2+}$  determination is shown in Fig. 2A. Owing to the specific interaction of  $\text{Hg}^{2+}$  and thymine,<sup>33–35</sup> and absence of thymine in A30 or B30, the fabricated disk cannot capture  $\text{Hg}^{2+}$ , subsequently resulting in no generation of AuNPs and oxTMB. Then, there is no change in the refractive index, further causing the SPR angle to shift slightly. Such an angle shift phenomenon can be quantitatively measured by the SPR technique. As shown in Fig. 2B, when A30 or B30 replaced T30 in the SPR sensor, the constructed assay displayed relatively low  $\Delta\theta$  values ( $0.036^\circ$  and  $0.028^\circ$  for A30,  $0.03^\circ$  and  $0.022^\circ$  for B30) when  $\text{Hg}^{2+}$  was present, which are smaller than that of the assay developed with T30. This difference indicates the stronger and more specific interactions of  $\text{Hg}^{2+}$  and thymine than

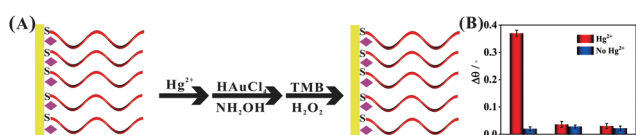


Fig. 2 (A) Diagram illustration of A30 or B30-based SPR sensor for  $\text{Hg}^{2+}$  assay. (B)  $\Delta\theta$  of the SPR sensors fabricated by T30, A30, and B30, respectively.

other bases. In addition, it is well acknowledged that  $\text{S}^{2-}$  has a stronger interaction force than thymine toward  $\text{Hg}^{2+}$ , and thus, it was inferred that  $\text{Hg}^{2+}$  in  $\text{Hg}^{2+}/\text{MCH}/\text{T30}/\text{Au}$  can be removed by  $\text{S}^{2-}$ . To confirm this, a pre-incubation experiment of  $\text{S}^{2-}$  with  $\text{Hg}^{2+}/\text{MCH}/\text{T30}/\text{Au}$  was conducted (Fig. S6, ESI†). Through this operation, the SPR sensor displayed the same angle as that of MCH/T30/Au, which is much smaller than that of the untreated sensor, implying no generation of AuNPs and oxTMB.

Further, the developed SPR sensor was employed to assay  $\text{Hg}^{2+}$  with different amounts to evaluate its sensing performance. To obtain the best response,  $\text{HAuCl}_4$  concentration,  $\text{NH}_2\text{OH}$  concentration, TMB concentration,  $\text{H}_2\text{O}_2$  concentration, and AuNP formation time were optimized (Fig. S7–S9, ESI†). At the optimized concentrations (0.5 mM, 20 mM, 0.2 mM, and 0.7 M) and reaction time (14 min), SPR characterizations were conducted. As shown in Fig. 3A and B, the SPR angle gradually increased with  $\text{Hg}^{2+}$  concentration elevating from 1 pM to 2000 pM, indicating a positive relation and conforming well to the working mechanism that more  $\text{Hg}^{2+}$  induced the generation of more AuNPs and more oxTMB. For quantitatively assessing the sensor's sensitivity, a working curve was drafted using  $\Delta\theta$  and the logarithm of  $\text{Hg}^{2+}$  concentration ( $\lg C_{\text{Hg}}$ ) as the ordinate and abscissa, respectively (Fig. 3C). Obviously,  $\Delta\theta$  was linearly related with  $\lg C_{\text{Hg}}$  with the range of 1–2000 pM, and the regression equation was calculated to be  $\Delta\theta = 0.09165 \lg C_{\text{Hg}} + 0.0694$  with a coefficient of 0.9892. In addition, the detection limit was determined to be 0.46 pM based on  $3\sigma$ . Compared with other reported  $\text{Hg}^{2+}$  sensors (Table S2, ESI†), our sensor enjoyed relatively high sensitivity, justifying the AuNP-assisted signal amplification efficiency. Moreover, the reproducibility was studied by fabricating five different MCH/T30/Au disks to develop SPR sensors. As illustrated in Fig. S10 (ESI†), the

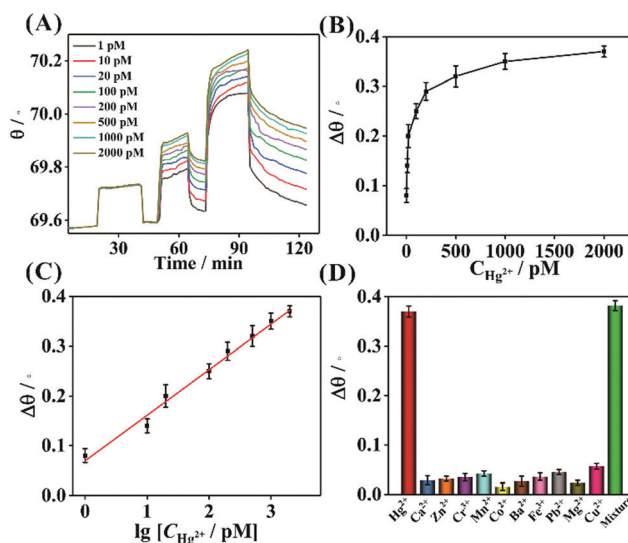


Fig. 3 (A) SPR curves corresponding to different  $\text{Hg}^{2+}$  concentrations. (B)  $\Delta\theta$  versus different  $\text{Hg}^{2+}$  concentrations. (C) Linear relationship between  $\Delta\theta$  and  $\lg C_{\text{Hg}}$ . (D) Specificity experiment of nanozyme-based SPR sensor for  $\text{Hg}^{2+}$ .

maximum angle change was only  $0.026^\circ$ , which is negligible, affirming the high reproducibility.

The selective response of the nanozyme-based SPR sensor to  $\text{Hg}^{2+}$  in the presence of other metal ions ( $\text{Ca}^{2+}$ ,  $\text{Cr}^{3+}$ ,  $\text{Zn}^{2+}$ ,  $\text{Mn}^{2+}$ ,  $\text{Co}^{2+}$ ,  $\text{Ba}^{2+}$ ,  $\text{Fe}^{3+}$ ,  $\text{Pb}^{2+}$ ,  $\text{Mg}^{2+}$ ,  $\text{Cu}^{2+}$ ) was studied, as shown in Fig. 3D. The angle of the SPR disk in the presence of one of the interfering ions was much lower than that in the presence of  $\text{Hg}^{2+}$ , indicating no formation of AuNPs and oTMB. At the same time, mixing these metal ions with  $\text{Hg}^{2+}$  caused a negligible effect on the output angle of the proposed SPR sensor toward target  $\text{Hg}^{2+}$ . This result suggested that only  $\text{Hg}^{2+}$  can induce the SPR angle to significantly increase due to the T- $\text{Hg}^{2+}$ -T coordination chemistry, justified the unique specificity for differentiating  $\text{Hg}^{2+}$  against other metal ions, and provided a promising tool for  $\text{Hg}^{2+}$  determination in environmental monitoring and assessment.

The practical application of the SPR sensor for  $\text{Hg}^{2+}$  was validated by carrying out measurements on tap water and lake water. No or only a slight increase in the angle was recorded in tap or lake water, suggesting that no  $\text{Hg}^{2+}$  existed. Then, both water samples were further analyzed by adding 10, 100, and 500 pM  $\text{Hg}^{2+}$  into the system, followed subsequently by a SPR test. The data in Table S3 (ESI<sup>†</sup>) demonstrated that the developed nanozyme-based SPR sensor had acceptable recoveries in the range of 97.2–109% and relatively low relative standard deviations (RSDs) ranging from 2.96% to 6.86%, justifying the significant potential for monitoring  $\text{Hg}^{2+}$  in complicated environmental samples.

In this work, a novel nanozyme-amplified SPR sensor for  $\text{Hg}^{2+}$  was developed based on target-induced *in situ* generation of AuNPs and a AuNP-guided cascade reaction. Compared with the previously reported SPR sensors, our sensor possessed some noteworthy advantages. (1) This was the first time an *in situ* generated nanozyme was applied for SPR sensor development. (2) It makes full use of the SPR effect and enzyme property of AuNPs to achieve highly sensitive biosensing of  $\text{Hg}^{2+}$ . (3) It avoided the complex/strict fabrication and modification conditions for AuNPs for the development of the SPR sensor. Thus, our sensor is simple and cost-effective, and can be applied in the analysis of  $\text{Hg}^{2+}$  in environmental samples with acceptable results. Furthermore, this strategy is applicable to other target analytes, which can remove  $\text{Hg}^{2+}$  from T- $\text{Hg}^{2+}$ -T through stronger bonds. We expect this study will not only provide a new path for the development of a high-performance SPR sensor, but will also enrich the signal amplification of other materials, which is favourable to broaden and deepen SPR sensor application.

This work was financially supported by the National Natural Science Foundation of China (21605093 and 21775082), the Shandong Province Higher Educational Program for Young Innovation Talents, the Major Program of Shandong Province Natural Science Foundation (ZR2018ZC0127), and the Special Foundation for Distinguished Taishan Scholar of Shandong Province (ts201511052).

## Conflicts of interest

There are no conflicts to declare.

## Notes and references

- H. H. Nguyen, J. Park, S. Kang and M. Kim, *Sensors*, 2015, **15**, 10481–10510.
- J. A. Jackman, A. Rahim Ferhan and N.-J. Cho, *Chem. Soc. Rev.*, 2017, **46**, 3615–3660.
- E. Zubritsky, *Anal. Chem.*, 2000, **72**, 289A–292A.
- J. F. Masson, *ACS Sens.*, 2017, **2**, 16–30.
- R. P. Gandhiraman, N. C. H. Le, C. K. Dixit, C. Volcke, C. Doyle, V. Gubala, S. Uppal, R. Monaghan, B. James, R. O'Kennedy, S. Daniels and D. E. Williams, *ACS Appl. Mater. Interfaces*, 2011, **3**, 4640–4648.
- Y. F. Chang, W. H. Wang, Y. W. Hong, R. Y. Yuan, K. H. Chen, Y. W. Huang, P. L. Lu, Y. H. Chen, Y. A. Chen, L. C. Su and S. F. Wang, *Anal. Chem.*, 2018, **90**, 1861–1869.
- J. F. Chang, X. Wang, J. Wang, H. Y. Li and F. Li, *Anal. Chem.*, 2019, **91**, 3604–3610.
- J. Ki, E. Jang, S. Han, M. K. Shin, B. Kang, Y. M. Huh and S. Haam, *ACS Appl. Mater. Interfaces*, 2017, **9**, 17702–17709.
- I. Ahmad, Z. Zhou, H. Y. Li and S. Q. Zang, *Sens. Actuators, B*, 2020, **304**, 127379.
- M. Singh, M. Holzinger, M. Tabrizian, S. Winters, N. C. Berner, S. Cosnier and G. S. Duesberg, *J. Am. Chem. Soc.*, 2015, **137**, 2800–2803.
- L. Wu, Y. Hu, Y. He, Y. Xia, H. Lu, Z. Cao, X. Yi and J. X. Wang, *Analyst*, 2019, **144**, 3959–3966.
- P. X. Yuan, S. Y. Deng, C. Y. Zheng, S. Cosnier and D. Shan, *Biosens. Bioelectron.*, 2017, **97**, 1–7.
- Q. Wang, L. Zou, X. Yang, X. Liu, W. Nie, Y. Zheng, Q. Cheng and K. M. Wang, *Biosens. Bioelectron.*, 2019, **135**, 129–136.
- X. Q. Li, Z. Zhou, C. C. Zhang, Y. H. Zheng, J. W. Gao and Q. M. Wang, *Sens. Actuators, B*, 2018, **276**, 95–100.
- P. He, W. Qiao, L. Liu and S. S. Zhang, *Chem. Commun.*, 2014, **50**, 10718–10721.
- Z. Lou, H. Han, M. Zhou, J. Wan, Q. Sun, X. Zhou and N. Gu, *Anal. Chem.*, 2017, **89**, 13472–13479.
- J. M. Lee, A. Hwang, H. Choi, Y. Jo, B. Kim, T. Kang and Y. Jung, *Angew. Chem., Int. Ed.*, 2017, **56**, 15998–16002.
- S. Zeng, D. Baillargeat, H. P. Ho and K. T. Yong, *Chem. Soc. Rev.*, 2014, **43**, 3426–3452.
- H. Y. Li, J. F. Chang, T. Hou and F. Li, *Anal. Chem.*, 2017, **89**, 673–680.
- X. Wang, T. Hou, H. Y. Lin, W. X. Lv, H. Y. Li and F. Li, *Biosens. Bioelectron.*, 2019, **137**, 82–87.
- Z. He, Y. Xiao, J.-R. Zhang, P. Zhang and J. J. Zhu, *Chem. Commun.*, 2018, **54**, 2962–2965.
- D. Jiang, D. Ni, Z. T. Rosenkrans, P. Huang, X. Yan and W. Cai, *Chem. Soc. Rev.*, 2019, **48**, 3683–3704.
- J. Wu, X. Wang, Q. Wang, Z. Lou, S. Li, Y. Zhu, L. Qin and H. Wei, *Chem. Soc. Rev.*, 2019, **48**, 1004–1076.
- S. Zhang, Z. Zhang, T. Wang, D. Zhang, X. Li, Z. Xue, D. Shan and X. Lu, *Chem. Commun.*, 2017, **53**, 5056–5058.
- Y. Lin, J. Ren and X. G. Qu, *Adv. Mater.*, 2014, **26**, 4200–4217.
- R. Takahata, S. Yamazoe, K. Koyasu and T. Tsukuda, *J. Am. Chem. Soc.*, 2014, **136**, 8489–8491.
- L. Hong, M. Lu, M. P. Dinel, P. Blain, W. Peng, H. Gu and J. F. Masson, *Biosens. Bioelectron.*, 2018, **109**, 230–236.
- W. Nie, Q. Wang, L. Zou, Y. Zheng, X. Liu, X. Yang and K. M. Wang, *Anal. Chem.*, 2018, **90**, 12584–12591.
- G. H. Yao, R. P. Liang, X. D. Yu, C. F. Huang, L. Zhang and J. D. Qiu, *Anal. Chem.*, 2015, **87**, 929–936.
- J. Li, W. Tu, H. Li, M. Han, Y. Lan, Z. H. Dai and J. Bao, *Anal. Chem.*, 2014, **86**, 1306–1312.
- H. Aoki, R. M. Corn and B. Matthews, *Biosens. Bioelectron.*, 2019, **142**, 111565.
- Z. Z. Sun, N. Zhang, Y. M. Si, S. Li, J. W. Wen, X. B. Zhu and H. Wang, *Chem. Commun.*, 2014, **50**, 9196–9199.
- R. Y. Wang, X. H. Zhou, H. C. Shi and Y. Luo, *Biosens. Bioelectron.*, 2016, **78**, 418–422.
- A. G. Memon, Y. P. Xing, X. H. Zhou, R. Y. Wang, L. H. Liu, S. Y. Zeng, M. He and M. Ma, *J. Hazard. Mater.*, 2020, **384**, 120948.
- A. G. Memon, X. H. Zhou, J. C. Liu, R. Y. Wang, L. H. Liu, B. F. Yu, M. He and H. C. Shi, *J. Hazard. Mater.*, 2017, **321**, 417–423.